Factors affecting O_3 and NO_2 photolysis frequencies measured in the eastern Mediterranean during the five-year period 2002–2006

E. Gerasopoulos,[1] S. Kazadzis,[1] M. Vrekoussis,[2,3] G. Kouvarakis,[4] E. Liakakou,[1] N. Kouremeti,[5] D. Giannadaki,[4] M. Kanakidou,[4] B. Bohn,[6] and N. Mihalopoulos[4]

Received 14 February 2012; revised 4 October 2012; accepted 7 October 2012; published 28 November 2012.

[1] The photolysis frequencies of ozone (O_3; to singlet oxygen, JO^1D) and nitrogen dioxide (NO_2; JNO_2) were recorded at the remote coastal site Finokalia (35°20′N, 25°40′E), on the island of Crete, Greece, during the period 2002–2006. We present a study of their main climatological aspects and a quantification of the effect of aerosol and total ozone column on these frequencies. The 5-yr mean Aerosol Optical Depth (AOD) at 380 nm in the area is equal to 0.27 ± 0.13 and reduces JNO_2 by 5%–14% at a solar zenith angle (sza) of 60°, compared to an aerosol-free atmosphere. It also leads to a similar reduction of JO^1D by 5%–15% at the 60° sza, for an average total ozone column (300–320 Dobson units (DU)). The effect of regional background AOD (∼0.1) is a reduction of JNO_2 and JO^1D by up to 6% for sza in the range 15° to75°, respectively. During high aerosol loads (AOD 0.5–0.7) the percentage reduction of Js was found to be as much as 30%–40% at high sza. The day-to-day variability of total ozone column over the area, of the order of 20 DU, was found to result in a 12% change in JO^1D at 60° sza as compared with zero AOD conditions. A reduction of Js corresponding to a 24% decrease in the local noon JO^1D value and a 5% decrease in local noon JNO_2 were found to result in a 12% reduction in the 24 h mean net chemical production of O_3, using a chemical box model.

Citation: Gerasopoulos, E., S. Kazadzis, M. Vrekoussis, G. Kouvarakis, E. Liakakou, N. Kouremeti, D. Giannadaki, M. Kanakidou, B. Bohn, and N. Mihalopoulos (2012), Factors affecting O_3 and NO_2 photolysis frequencies measured in the eastern Mediterranean during the five-year period 2002–2006, *J. Geophys. Res.*, *117*, D22305, doi:10.1029/2012JD017622.

1. Introduction

[2] Atmospheric chemistry of importance for climate change, visibility, human's and ecosystem's health, is partly controlled by the photolysis of atmospheric trace gases. This process initiates the degradation of several atmospheric tracers and is at the origin of oxidant formation which determines the cleaning capacity of the atmosphere [*Crutzen*, 1995]. In particular, UV radiation drives the photolysis of several critical species, such as O_3 and NO_2, controlling their decomposition and removal from the atmosphere. The photolysis of O_3 to singlet oxygen atoms O^1D (JO^1D), determines the formation of highly reactive radicals such as hydroxyl-OH and hydroperoxyl-HO_2 radicals [*Rohrer and Berresheim*, 2006; *Kraus and Hofzumahaus*, 1998], which in turn are essential for tropospheric ozone concentrations [*Dickerson et al.*, 1997; *He and Carmichael*, 1999; *Zanis et al.*, 2002; *Li et al.*, 2011].

[3] Indeed, the photolysis of tropospheric O_3 to O^1D and the subsequent reaction of O^1D with water vapor is the principal global source of OH radicals. The oxidation of carbon monoxide (CO) and volatile organic compounds (VOC) mainly initiated by OH radicals produces HO_2 and organic peroxy (RO_2) radicals [*Kanakidou and Crutzen*, 1999]. These radicals convert nitric oxide (NO) to nitrogen dioxide (NO_2) thus binding oxygen (O^3P) atoms to NO_2 which are then released upon NO_2 photodissociation and recombination with molecular O_2 to form O_3. At very high levels of NO_x ($NO + NO_2$), NO reacts with O_3 to produce NO_2 that acts as a sink for OH, limiting VOC and CO oxidation and hence O_3 formation [*Crutzen*, 1995; *Finlayson-Pitts and Pitts*, 2000]. Similarly, at low levels of NO_x, O_3 is

[1]Institute for Environmental Research and Sustainable Development, National Observatory of Athens, Athens, Greece.
[2]Research Centre for Atmospheric Physics and Climatology, Academy of Athens, Athens, Greece.
[3]Now at Energy, Environment and Water Research, Cyprus Institute, Nicosia, Cyprus.
[4]Environmental Chemical Processes Laboratory, Chemistry Department, University of Crete, Heraklion, Greece.
[5]Laboratory of Atmospheric Physics, Physics Department, Aristotle University of Thessaloniki, Thessaloniki, Greece.
[6]Institute of Energy and Climate Research, Jülich, Germany.

Corresponding author: E. Gerasopoulos, Institute for Environmental Research and Sustainable Development, National Observatory of Athens, Metaxa and Vas. Pavlou, Penteli, GR-15236 Athens, Greece. (egera@meteo.noa.gr)

0148-0227/12/2012JD017622

not produced in the troposphere, and reactions of O_3 with OH and HO_2 radicals and the formation of organic peroxides are important. To account for these nonlinear dependences of OH on NO_x, *Ehhalt and Rohrer* [2000] have proposed a parameterization that links OH radical concentration with the two most important photolysis frequencies JO^1D and JNO_2 in conjunction with NO_2 concentration.

[4] The important role of photolysis and the need for accurate photolysis frequencies measurements has been early recognized [*Bahe et al.*, 1979; *Dickerson et al.*, 1979]. Since the 1990s, calculations of photolysis frequencies have been based on direct measurements of spectral actinic flux [e.g., *Müller et al.*, 1995]. This led to numerous campaigns that were totally or partly devoted to methodologies, monitoring and the investigation of those factors that affect the variability of photolysis frequencies (e.g., POPCORN [*Plass-Dülmer et al.*, 1998], PAUR [*Zerefos et al.*, 1998], FREETEX'96 [*Zanis et al.*, 1999], FREETEX'98 [*Zanis et al.*, 2000], ATOP [*Hofzumahaus et al.*, 2002], PAUR II [*Zerefos et al.*, 2002], ADMIRA [*Webb et al.*, 2002], BERLIOZ [*Holland et al.*, 2003], IPMMI [*Bais et al.*, 2003], TRACE-P [*Jacob et al.*, 2003], MILAGRO [*Molina et al.*, 2010]). The most important parameters controlling photolysis frequencies are: solar zenith angle (sza), clouds, aerosols (optical depth, single scattering albedo), species column content, surface albedo and the altitude. *Ruggaber et al.* [1994] provide a model-based quantification of the influence of the above parameters on photolysis frequencies.

[5] The photolysis (or photodissociation) frequency J of a species is the first-order rate constant of a photodissociation process in a given radiation field. It is described by the following equation [e.g., *Madronich*, 1987]:

$$J = \int_{\lambda 1}^{\lambda 2} F(\lambda)\sigma(\lambda, T)\Phi(\lambda, T)d\lambda \quad (1)$$

where $\sigma(\lambda, T)$ (cm^2) is the absorption cross section of the species that absorbs in the wavelength range $\lambda_1 - \lambda_2$, $\Phi(\lambda, T)$ is the quantum yield of the photodissociation reaction product, and $F(\lambda)$ is the spectral actinic flux density. In particular, JO^1D is proportional to $F(\lambda)$ (equation (1)) at wavelengths smaller than 340 nm, mainly from 305 to 325 nm where ozone absorbs, and $\Phi(\lambda, T)$ is high (between 0.9 and 0.1 at 298 K) [e.g., *Atkinson et al.*, 2004]. For the photolysis frequency of NO_2 to O^3P that leads to O_3 formation (JNO_2), wavelengths shorter than 420 nm and mainly from 365 to 390 nm are important, where there is practically no ozone absorption band and quantum yields are unity at 298 K [e.g., *Atkinson et al.*, 2004; *Topaloglou et al.*, 2005].

[6] The spectral actinic flux density is the total number of photons per wavelength unit incident on the molecules of the species in the atmosphere:

$$F(\lambda) = F_d(\lambda) + F_0(\lambda) = \int_0^{2\pi}\int_0^{\pi} I(\lambda, \theta, \varphi)\sin(\theta)\ d\theta d\varphi \quad (2)$$

where F_o is the direct and F_d the diffuse spectral actinic flux density incident on the molecule of the atmospheric species in question, I is the spectral sky radiance (including the direct Sun component), θ is the zenith angle and φ is the azimuth angle. For measurements of the spectral actinic flux density only for the upper hemisphere, the upper limit of the integral over θ is $\pi/2$ (equation (2)).

[7] The Mediterranean, and especially its eastern basin, is a photochemically very active region. It experiences a high background of tropospheric ozone [e.g., *Gerasopoulos et al.*, 2005, 2006] and a mixing of high aerosol concentrations of various origin and characteristics [e.g., *Querol et al.*, 2009]. It also experiences significant changes in total ozone column since it is located at the edge of the subtropics. Thus tropical and polar ozone regimes are succeeded over the region [*Hudson et al.*, 2003]. The combined effect of aerosols and total ozone column over the eastern Mediterranean can be quite complex since, even under conditions of reduced total ozone column, the high levels of tropospheric ozone and absorbing dust aerosols, can still cause a substantial decrease in the photolysis frequencies of ozone [*Zerefos et al.*, 2002].

[8] Apart from devoted campaigns, long-term measurements of photolysis frequencies in the central/eastern Mediterranean do not exist. Most have been limited to shorter periods of time, of the order of a few months, or have been confined to several nonconsecutive periods taken from different years, or have been based on empirical/indirect retrieval approaches [*Kazadzis et al.*, 2004; *Topaloglou et al.*, 2005; *Casasanta et al.*, 2011].

[9] Some basic characteristics of a small part of these photolysis frequencies data series used in the present work have been reported by *Gerasopoulos et al.* [2006], for the investigation of photochemical ozone production in the area. The first long-term (2002–2006) measurements in the eastern Mediterranean of JO^1D and JNO_2 are presented here, together with a climatological analysis of the photolysis frequencies record and investigation of the role of aerosols and total ozone column on the Js variability.

2. Measurements and Methods

2.1. Location

[10] The total solar radiation and photolysis frequencies (JO^1D, JNO_2) were measured at Finokalia (35°20′N, 25°40′E; http://finokalia.chemistry.uoc.gr), a remote coastal site in the northeast part of the island of Crete, Greece, in the eastern Mediterranean (an operational site of Aerosols, Clouds, and Trace gases Research Infrastructure Network (ACTRIS)). The Finokalia station is situated 70 km east of Heraklion, the island's biggest city with a population of about 140 k inhabitants. The site and its prevailing meteorology have been previously described by *Mihalopoulos et al.* [1997]. The Finokalia data are analyzed here together with aerosol optical properties data taken from the FORTH-CRETE AERONET station which is located on the roof of the Cretan National Center for Marine Research, 20 m above sea level, 100 m inland from the coast, and 50 km to the west of Finokalia.

2.2. Instrumentation

[11] Measurements of JNO_2 and JO^1D were performed by 2π commercially available filter radiometers (Meteorologie Consult, Metcon, Germany) during the period 2002–2006. In brief, quartz receivers were used for the collection of the 2π radiation (only upper hemisphere); optical filters for wavelength separation, and phototubes or photomultipliers for detection [e.g., *Junkermann et al.*, 1989; *Volz-Thomas et al.*, 1996]. Both instruments provided an output analog

voltage signal, which was averaged and recorded on a data logger with a time resolution of 5 min. The detected signal was converted to photolysis frequency using the response function of each instrument. The sensors were calibrated four times during the study period (2002, 2003, 2005 and 2006) against a spectral radiometer at Forschungszentrum Jülich, Germany. The calibration of the JNO_2 instrument follows a straightforward procedure whereby a calibration factor is used to convert the output voltages to photolysis frequencies after subtracting the background [*Bohn et al.*, 2008]. Conversely, the calibration of the JO^1D output is more complicated because the solar spectrum variability in the UV-B spectral region depends on the ozone column content and the sza [*Hofzumahaus et al.*, 2004]. A computational routine provided by the manufacturer using an updated correction function together with the calibration factors has been applied. This routine accounts for the solar zenith angle as well as the total ozone column [*Bohn et al.*, 2004]. The updated correction function is based on a spectral characterization of the instrument in 2006 that led to a retroactive improvement compared to the 2005 status documented previously [*Bohn et al.*, 2008]. Both Js were corrected for the Sun-Earth distance and a correction for the effect of the ambient temperature on JO^1D was applied according to *Bohn et al.* [2004]. The total ozone column was obtained by TOMS (Total Ozone Mapping Spectrometer) in the period up to 2005 and OMI (Ozone Monitoring Instrument) for the year 2006, using overpass data. Overall, the accuracy of Js measurements is estimated to be 15% (1 sigma), at sza < 75° [see *Bohn et al.*, 2008]. Total solar radiation measurements were also performed at Finokalia using a pyranometer CM3 (Campbell Scientific, Inc.).

[12] Aerosol optical properties measured with a CIMEL Sun photometer (AERONET level 2 data collection, http://aeronet.gsfc.nasa.gov/) at FORTH-CRETE AERONET station, have also been used. The CIMEL Sun photometer is an automatic Sun-sky scanning radiometer using selected spectral channels. The instrumentation, data acquisition, retrieval algorithms and calibration procedure conform to the standards of the AERONET global network, and are described in detail by *Fotiadi et al.* [2006]. The overall uncertainty in AOD data, under cloud-free conditions, is 0.02 at a wavelength of 380 nm [*Dubovik and King*, 2000].

2.3. Methodology for Cloud Screening

[13] For the detection of periods where clouds were not present in front or around the solar disk, the shape of the diurnal course of total solar radiation, recorded by the pyranometer every 5 min, is examined. To eliminate cases of overcast skies or the presence of broken clouds that lead to enhancement of solar radiation, radiation values were selected that fell within the limits obtained from clear-sky solar irradiance calculations with the LibRadTran Radiation Transfer code [*Mayer and Kylling*, 2005]. The limits represent cloudless cases of high and no aerosol load, based on aerosol optical depth measurements. For the remainder of the data, a comparison of measured and modeled solar irradiances with respect to sza at 1° intervals, was performed. This procedure examines each 5 min measurement within a time window of 30 min centered on the time of each measurement. For each time window the criteria that were examined are: the absolute difference between measured and modeled radiation, and the relative change of measured solar radiation. The latter includes a quantification of the sza change and the effect of the presence of cirrus clouds. When all the above criteria pass predefined empirical thresholds, then the minute examined is flagged as a clear-sky Sun measurement.

2.4. Box Model Description

[14] The box model used in this study has been previously described by *Poisson et al.* [2001], *Tsigaridis and Kanakidou* [2002], *Vrekoussis et al.* [2004] and *Gerasopoulos et al.* [2006]. For the present study, observed 5 min values of O_3, CO, NO, JNO_2, JO^1D, temperature, relative humidity (RH) and wind speed are used as input to the chemical box model. NO_2 nighttime values measured by DOAS [*Vrekoussis et al.*, 2006] are also used as input to the model. Isoprene, ethene, propene, ethane, propane and butane mixing ratios were based on measurements performed in the area (February–October 2004 [*Liakakou et al.* [2007, 2009]) and in the western Mediterranean [*Plass-Dülmer et al.*, 1992]. No direct heterogeneous ozone losses are included in the model whereas NO_2, N_2O_5, HO_2 and RO_2 heterogeneous losses are parameterized as described by *Tsigaridis and Kanakidou* [2002] and *Vrekoussis et al.* [2004]. As described by *Gerasopoulos et al.* [2006, and references therein], the net chemical production of O_3 was computed as the difference between the chemical production (P_{O3}) and the chemical destruction (L_{O3}) of O_3. P_{O3} was derived as the sum:

$$P_{O_3} = \sum R_{RO_2NO}[RO_2][NO] \quad (3)$$

for all peroxy radicals (RO_2), including hydrogen peroxide (HO_2) and reactions with NO to form NO_2, whereas L_{O3} was computed as the sum of the losses of O_3 from (1) photolysis to O^1D and reaction with water vapor to form OH radical, (2) reactions of O_3 with HO_x (OH and HO_2), and (3) reactions with unsaturated volatile organics and sulfur compounds.

2.5. Radiative Transfer Model Description

[15] The radiative transfer model LibRadTran [*Mayer and Kylling*, 2005] was used to calculate the spectral solar actinic flux in the wavelength range 290–450 nm with a spectral resolution of 0.5 nm. For the parameterization of the atmosphere we used the following: synchronous (±15 min from each photolysis frequency measurement) aerosol properties taken from the AERONET Level 2 (CIMEL Sun photometer), the atlas plus modtran [*Mayer and Kylling*, 2005] extraterrestrial spectrum, rural type aerosols according to *Shettle* [1989], the standard atmosphere profile from U.S. atmosphere [*Anderson et al.*, 1986], total columnar ozone from the OMI satellite and the sza for each photolysis measurement. For the calculation of the O^1D and NO_2 photolysis frequencies the quantum yields from *Matsumi et al.* [2002] and *Troe* [2000] were used, respectively. In addition, ozone cross sections from *Malicet et al.* [1995] and NO_2 cross sections from *Vandaele et al.* [2003] were used. The radiative transfer model outputs allowed

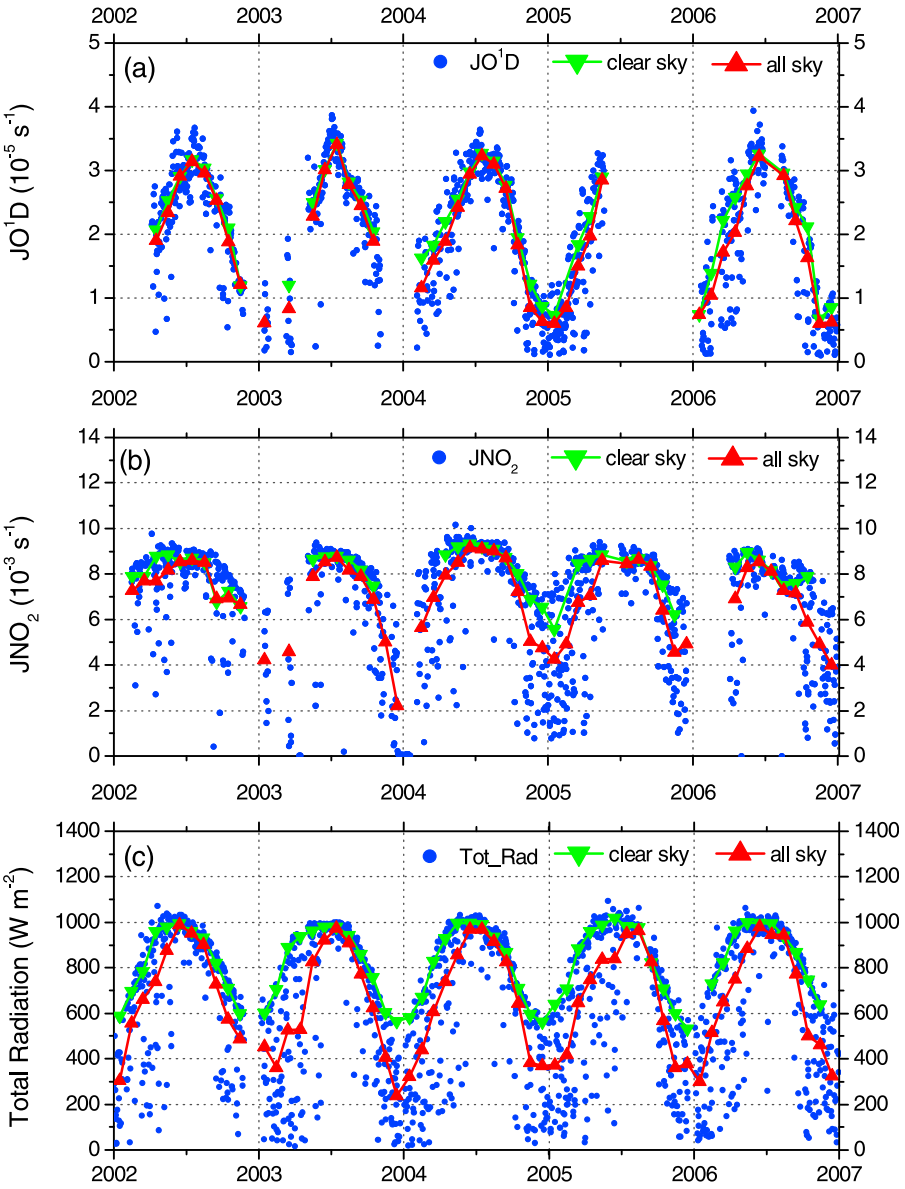

Figure 1. Time series of the photolysis frequencies of (a) O_3 (JO^1D) and (b) NO_2 (JNO_2) and (c) total solar radiation. Daily values refer to local noon for the period 2002–2006. Red and green triangles correspond to all-sky and clear-sky conditions and are calculated as monthly means from daily local noon values.

a photolysis frequency for the time of each measurement to be calculated.

3. Results

3.1. Climatological Aspects of Photolysis Frequencies

3.1.1. Data Presentation: Local Noon Values

[16] The photolysis frequencies of O_3 and NO_2 as well as the total radiation at local noon, for a time span of 5 yrs covering the period 2002–2006, are presented in Figure 1. The complete series is denoted as "all sky" while the subset "clear sky" includes all those values not affected by clouds. Basic statistics on all-sky, daily values of both Js and the total radiation are provided in Table 1. Gaps in the data series are related to instrument calibration, participation in campaigns elsewhere or malfunction. They account mostly for winter time data and they result to an overestimation of the whole period means by 4% for JNO_2 and 8% for JO^1D, which is well within the standard deviation of the mean values.

Table 1. Basic Statistical Quantities for JO^1D, JNO_2, and the Total Solar Radiation

	All Sky Local Noon Values		
	JO^1D (10^{-5} s^{-1})	JNO_2 (10^{-3} s^{-1})	Total Radiation (W m^{-2})
Avg ± SD	2.1 ± 1.0	7 ± 2.4	668 ± 300
Max	3.9	10.2	1096
75th percentile	2.9	8.7	942
Median	2.3	8.0	738
25th percentile	1.2	6.1	437

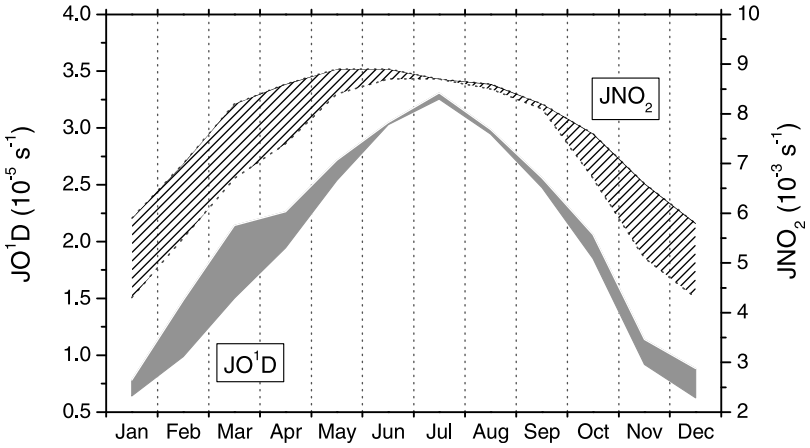

Figure 2. Whole period local noon averaged seasonal cycles of the photolysis frequencies of O_3 (JO^1D) and NO_2 (JNO_2). The upper and lower limits of the shaded areas correspond to clear-sky and all-sky data.

[17] For both photolysis frequencies, the interannual variability of their maximum, clear-sky monthly means is of the order of 7%–8%, while for the total radiation it is 4%. No particular trends are observed in the time series.

3.1.2. Seasonal Variability

[18] The seasonal variability of the local noon values of photolysis frequencies is presented in Figure 2. A much broader pattern is revealed for JNO_2 than for JO^1D. Higher JNO_2 values ($8.9 \cdot 10^{-3}$ s^{-1}) are observed during May–June. In contrast, JO^1D presents an abrupt maximum of $3.2 \cdot 10^{-5}$ s^{-1} in July. The seasonality is mainly driven by the change of the incident angle of solar radiation. In addition, both photolysis frequencies levels depend on clouds and aerosols, while in the case of JO^1D, the total ozone column plays a significant role. This is due to the dependence of JO^1D on (mainly stratospheric) ozone absorption, while JNO_2 is negligibly affected by total ozone column. The effect of total ozone column on JO^1D and of aerosols on both Js, depends not only on the columnar content, but also on the length of the atmospheric path of the incident actinic flux which is proportional to 1/cos(sza).

[19] Thus, the higher rate of change of JO^1D compared to that of JNO_2 (Figure 2) is related to more efficient absorption by total ozone and stronger Rayleigh scattering at high sza's (longer atmospheric paths). A JNO_2 maximum is observed as June approaches, as expected due to dependence on sza. The JO^1D annual maximum is shifted to July due to the reduction of total O_3 column from June to July. Due to the strong dependence of JO^1D on both total O_3 column and sza, the seasonal variability of JO^1D is denoted with a max/min ratio of 3.8, whereas JNO_2 shows a weaker seasonal variability with a max/min ratio of 1.5.

3.1.3. Diurnal Variability

[20] The diurnal cycles of the photolysis frequencies per season are presented in Figure 3. JO^1D and JNO_2 follow different diurnal courses. For the particular analysis we selected to use the calendar instead of the astronomical seasons, as the discussion about the sza dependence of

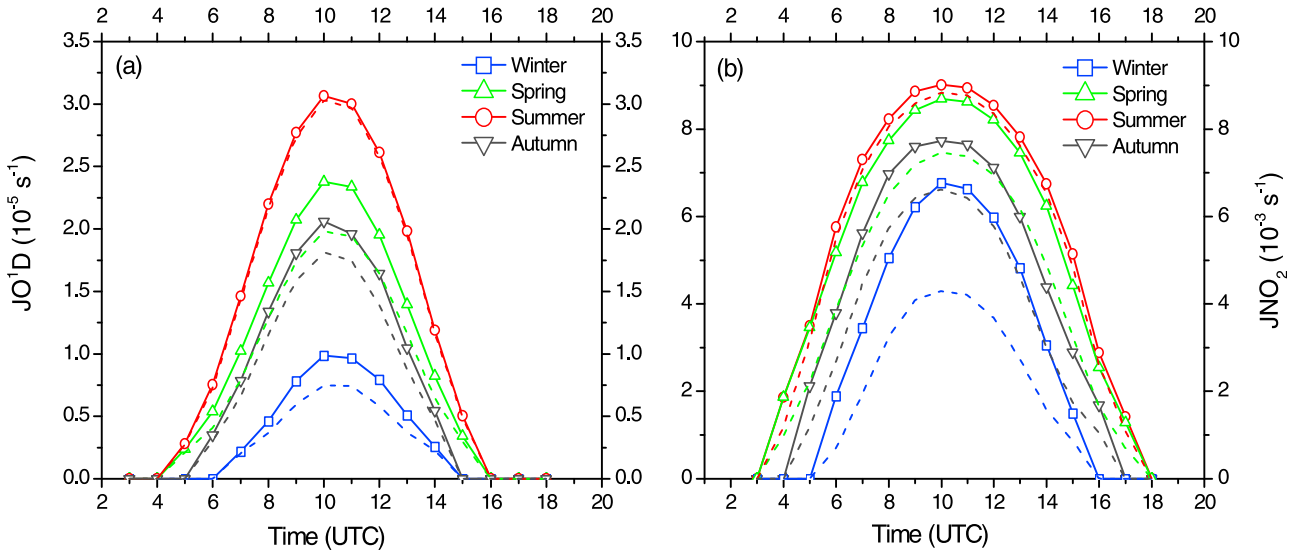

Figure 3. Whole period averaged diurnal cycles of the photolysis frequencies of O_3 (JO^1D) and NO_2 (JNO_2). Diurnal cycles are provided per season, solid lines (with symbol) correspond to clear-sky, and dashed lines correspond to all-sky data.

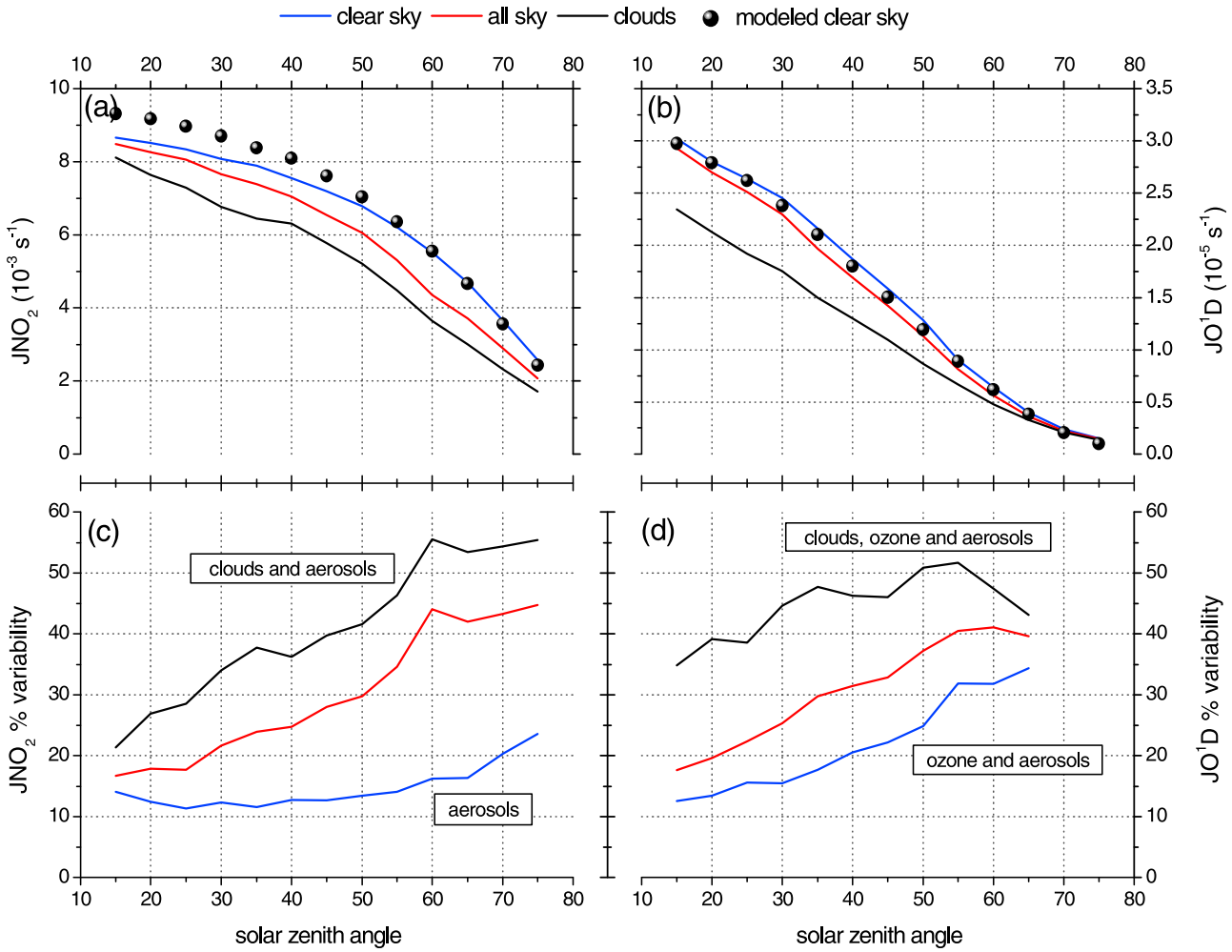

Figure 4. Whole period averaged photolysis frequencies of (a) NO_2 (JNO_2) and (b) O_3 (JO^1D), versus the solar zenith angle (sza), for all-sky, clear-sky and cloudy (defined just subtracting cloudless from all-sky) conditions. Mean values of Js are calculated every 5 degrees of sza (±0.5 degrees). (c, d) Js variability expressed as the ratio of the standard deviation of Js to their mean value, per 5 degree sza bin. Modeled values were derived from the radiative transfer model LibRadTran.

photolysis frequencies is provided in section 3.2.3. During the first hours after sunrise and before sunset (high sza's) the JO^1D rate of change is higher than that of JNO_2. This is again due to a rapid increase in the length of the optical path covered by the incident solar actinic flux in the atmosphere as sza increases and thus in the absorption of this flux by total ozone. Concerning the diurnal maximum of JO^1D, it is encountered in summer due to sza effects and columnar ozone concentrations, which are both lower in summer compared to spring. For JNO_2, the two parameters that control its diurnal course are the sza and aerosols. Since the effect of aerosols in the area is maximized in summer (see also Figure 5), the difference of the diurnal maximum between summer and spring is less profound than for JO^1D clear-sky cases. The similarity of clear-sky and all-sky data during summer is characteristic for the area since cloudless conditions dominate. Conversely, there is a more significant difference in the wintertime when the effect of clouds is at a maximum.

3.2. Factors Controlling the Variability of Photolysis Frequencies

[21] The dependence of photolysis frequencies on the sza is shown in Figures 4a and 4b, for all-sky, clear-sky and cloudy (determined by subtracting cloudless from all-sky) conditions. Mean values of Js per 5 degrees of sza (±0.5 degrees) are presented. Once more it is evident that the rate of change of photolysis frequencies with sza is higher for JO^1D than for JNO_2. It should be noted that the data presented here for lower sza are biased by summer time values, while as sza increases, the representation of all seasons is gradually enhanced. It is also worth noting that at higher sza, the three JO^1D lines converge to values close to zero. Overall, the comparison between clear-sky and cloudy-sky cases shows that the mean J's attenuation by clouds ranges from 10% to 35%.

[22] In order to evaluate how such a long-term series of observations scales with respect to clear-sky values from a radiative transfer model, we have included in Figures 4a and

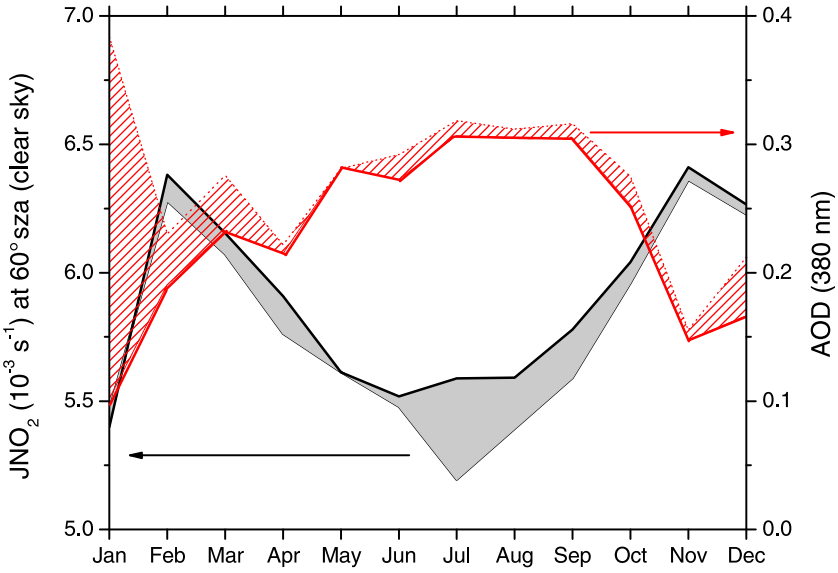

Figure 5. Seasonal cycles of the clear-sky photolysis frequency of NO_2 (JNO_2) at 60° sza and AOD (380 nm). The thick line limit of the shaded areas corresponds to median values, and the dotted line corresponds to mean values.

4b the LibRadTran model calculations for the same sza bins. The mean difference between model and measured values is of the order of 3% for JO^1D and 5% for JNO_2 (up to 8% for sza < 30°). Given the absolute calibration, measurement uncertainty and the uncertainties in input model parameters, it is concluded that there exists a good agreement between observations and model calculations.

[23] In order to investigate the variability of the photolysis frequencies and its dependence on various factors, we calculated and present in Figures 4c and 4d, the ratio of the standard deviation of the photolysis frequencies to their mean value, for each 5 degree sza bin. In the case of clear-sky data, the variability of JNO_2 for a given sza is mainly controlled by aerosols. For sza between 15° and 75°, this variability changes slightly, ranging from 10% to 25% (Figure 4c). The effect of a total column ozone increase of 200 DU on JNO_2 has been simulated and found to be less than 2% [*Ruggaber et al.*, 1994]. On the contrary, for JO^1D, there is a steady increase in variability with sza. By assuming that aerosols had a similar effect on both photolysis frequencies, then for JO^1D the additive effect of O_3 absorption is of the order of 20% at sza 55°–65° (Figure 4d). We attribute this steady increase to the combined effect of higher representation of all seasons at high sza's and the natural annual variability of total ozone column.

[24] JNO_2 cloudy cases vary from about 20%–30% at lower sza up to 55% at higher sza, while for JO^1D the range is between 35% and 55%. The higher variability in the Js under cloudy conditions compared to clear-sky cases results from the impact of various cloud fractions and types on the incident solar radiation. The increase with sza is linked to the different representation of seasons to each sza bin (lower sza's represent only summertime meaning fewer cloudy cases). The falling branch in the JO^1D change in variability with sza, seen at high sza (Figure 4d), cannot be interpreted because J values measured at such sza's are close to the instrument's detection limit due to the effect of high ozone absorption.

3.2.1. Aerosol Effects

[25] Many international studies have focused on the effects of various aerosol types on photolysis frequencies [e.g., *Jacobson*, 1998; *Liao et al.*, 1999; *Bian and Zender*, 2003; *Liao et al.*, 2003; *Li et al.*, 2011]. They indicate the different impact between absorbing and nonabsorbing aerosols on J's levels. The eastern Mediterranean atmosphere, receiving intensive solar radiation all year-around, is also characterized by a high concentration of aerosols of different origin and properties. Aerosol characteristics depend on long-range transport and on local sources that both show strong seasonal behavior. During summer, transport is driven by northerly winds and results in high loadings of anthropogenic particles. In spring the contribution of Saharan dust dominates although it happens on an "episodic" basis when dust outbreaks from Africa occur [e.g., *Gerasopoulos et al.*, 2011]. Thus, the eastern Mediterranean is an ideal place to investigate the role of various factors and, in particular, various types of aerosols, on photolysis frequencies.

[26] For this study, the AOD at 380 nm (provided by AERONET) was used as a proxy for aerosol loading over the region. This wavelength was selected as it is more representative of JNO_2. To eliminate the sza effect on Js so as to focus solely on aerosol effects during the entire 5-yr period, the following analysis focuses on a specific sza bin, 60° ± 1°. This sza equals the latitude of the measurement site plus the winter solstice declination of the Sun, accounts for the minimum sza encountered year-round, and has been chosen to eliminate biases on the results that arise from the strong seasonal variation of aerosols in the area [e.g., *Fotiadi et al.*, 2006].

[27] Figure 5 presents the annual cycle of clear-sky JNO_2 at 60° sza and that of AOD at 380 nm. Observation of the monthly mean or median values of the two parameters

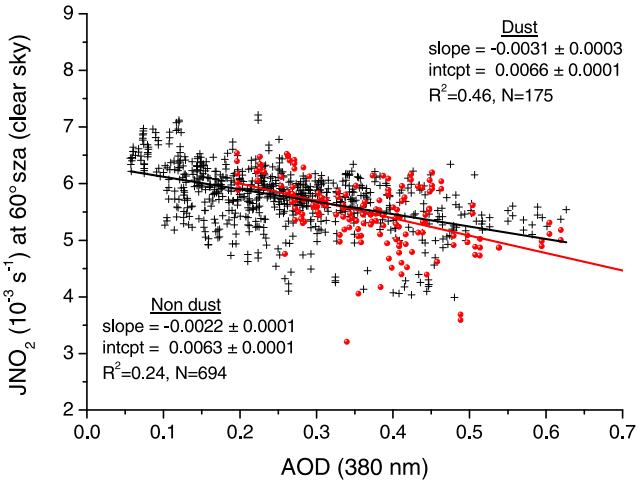

Figure 6. Photolysis frequency of NO_2 (JNO_2) at sza 60° (clear-sky data) versus the AOD (380 nm) are indicated by crosses. Dust episodes (red circles) selected by the AOD > 0.2 and Angström Exponent ($AE_{340/440}$) < 1 criteria are separately shown. Linear regression analysis information is included for both cases.

reveals a clear anticorrelation. Maximum aerosol loading occurs during summer inducing the lowest annual JNO_2 values at 60°. The widths of the shaded areas represent episodes of high aerosols of anthropogenic origin during summer. During spring and winter, they correspond to either frequent or intense Saharan dust outbreaks, respectively.

[28] To quantify the impact of aerosols on JNO_2, we plotted JNO_2 at 60° sza versus the AOD at 380 nm (Figure 6). In addition, we distinguished between dust episodes from other (non-Saharan dust) aerosol particles. The criteria used to mark the presence of dust were: an AOD > 0.2 and an Angström Exponent between 340 and 440 nm ($AE_{340/440}$) < 1. Under aerosol-free conditions (AOD = 0) the JNO_2 value at 60° is estimated to be $6.3 \cdot 10^{-3}$ s^{-1} and we found that 24% of JNO_2 variability can be explained by aerosol variability alone (it should be noted that part of the scattering of the points might be due to the 50 km distance between the Js and AOD measuring sites). The respective slope of the linear regression indicates a reduction of JNO_2 by $2.2 \cdot 10^{-3}$ s^{-1} per AOD unit. This translates to a percentage reduction of about 10% at 60° sza, under typical urban conditions (mean AOD_{380} = 0.3 extrapolated from *Gerasopoulos et al.* [2011]), and about 5% under regional background conditions (mean AOD_{380} = 0.13 extrapolated from *Fotiadi et al.* [2006]).

[29] Dust aerosols appear to contribute to JNO_2 variability (46%) significantly more than the nondust aerosols. The respective slope is 1.5 times higher than that of nondust aerosols, indicating a reduction of JNO_2 by $3.1 \cdot 10^{-3}$ s^{-1} per dust AOD unit. This translates to a percentage reduction of about 20% at 60° sza, under average dust loadings over the area (mean AOD_{380_dust} = 0.4 extrapolated from *Gerasopoulos et al.* [2011]). The higher slope for dust particles is due to the absorbing character (relatively low single scattering albedo) of dust [e.g., *Balis et al.*, 2004]. *He and Carmichael* [1999] found that desert aerosols cause the largest decrease in photolysis frequencies, due to their backscattering and strongly absorbing properties. Similarly, *Liao et al.* [1999] calculated that desert dust reduces photolysis frequencies at all altitudes below the dust layer, with the largest reduction occurring inside the dust layer. However, despite the fact that the statistical errors of the slopes presented in Figure 6 provide evidence of enhanced absorption due to dust, the measurement uncertainties make this conclusion mainly qualitative.

[30] To investigate the impact of aerosols on JO^1D, we have plotted JO^1D at 60° sza versus the AOD (dust and nondust cases) at 380 nm (Figure 7), for different total columnar ozone bins of width 20 DU. For total columnar ozone 300–320 DU, the slope is $-2.44 \cdot 10^{-6}$ s^{-1} per AOD unit. This translates to a percentage reduction of about 10% at 60° sza under typical urban conditions, and about a 4% reduction under regional background conditions. For the overall range of total ozone columns over the region (260–400 DU), the changes in JO^1D per AOD unit were found to lie in the range $-1.4 \cdot 10^{-6}$ to $-3.8 \cdot 10^{-6}$. At Lambedusa Island in the central Mediterranean [*Casasanta et al.*, 2011], the respective slopes (for AODs at 416 nm) at 60° sza ranged from $-2.6 \cdot 10^{-6}$ to $-5.8 \cdot 10^{-6}$. Taking into account the different AOD wavelength in the two studies, the results are in relatively good agreement (within 30% in the range 280–310 DU and within 10% in the range 310–340 DU).

[31] Despite the scatter of the data points for each ozone bin presented in Figure 7, it is worth noting that the change of JO^1D per AOD unit (dust and nondust cases) linearly decreases with increasing total ozone column. This is an expected scaling effect. Absorption in the ozone layer will reduce the radiation incident at the top of the aerosol layer (intercept values for AOD = 0). Then, the same relative attenuation by aerosols is encountered within all ozone bins, assuming a standard mixture of aerosols. The ratios of the calculated slopes to the respective intercept values range between 30% and 40%. There still remains a linear decrease of these ratios with increasing total ozone column, even though the trend is not statistically significant due to large associated errors. This could be probably linked to synoptic meteorological patterns that result to dominance of different types of aerosols over others. As analyzed by *Hudson et al.* [2003], when total ozone column is low, tropical O_3 regime affects the area. This is expected to be associated with transport of dust aerosol to the region from Africa. *Balis et al.* [2002] showed that highly absorbing aerosol loads associated with dust transport from the south can counterbalance the expected increase in UV radiation due the total ozone decrease or can even lead to a decrease in UV radiation. The reported values at Lambedusa [*Casasanta et al.*, 2011] show steeper trend of the ratios (slope/intercept) possibly reflecting a higher dust impact at this site. Such a pattern is not seen at 30° sza since the effects of aerosols and total ozone are lower, and thus they might be masked by the uncertainty in the slope's estimation.

3.2.2. Total Ozone Effects

[32] Figure 8 presents the annual cycle of clear-sky JO^1D at 60° sza together with that of total ozone column. A distinct anticorrelation is revealed, with the narrow total ozone maximum in spring being reflected as a broader minimum on JO^1D due to the additive effect of aerosols. JO^1D correlates with the change in total ozone column during fall-winter as aerosol levels at this time are at their minimum.

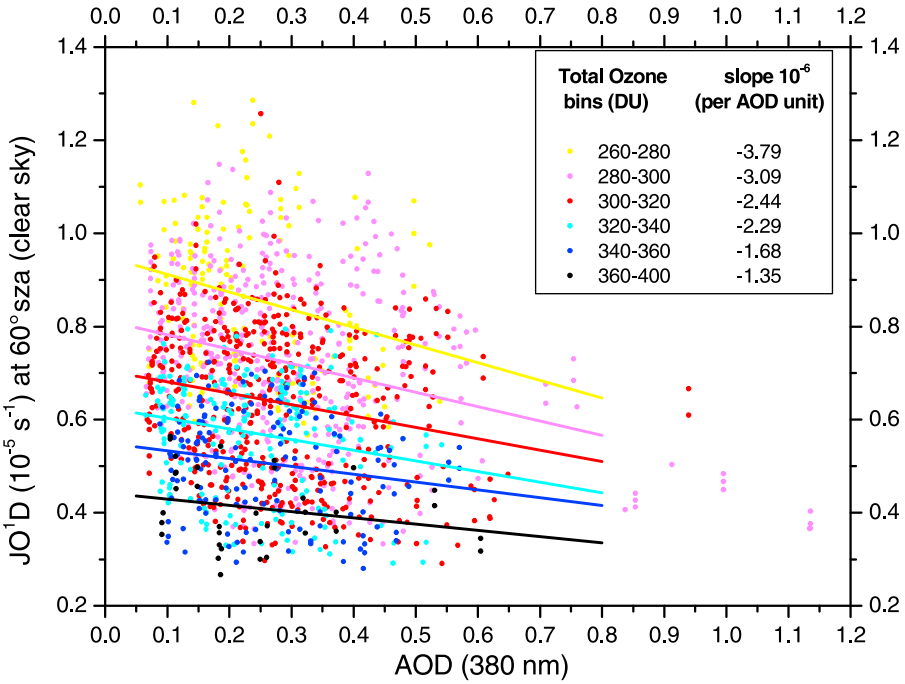

Figure 7. Photolysis frequency of O_3 (JO^1D) at 60° sza (clear-sky data) versus the AOD (380 nm), for different total ozone bins. Slopes per each total ozone bin are provided in the embedded table (regression analyses significant at the 95% confidence level in all cases except the 360–400 ozone bin).

[33] In Figure 8 the mean monthly ambient temperature correction on JO^1D is also included. The correction throughout the year has a maximum in the summer (3%) and minimum in the winter season (−7%). We have decided to apply the temperature correction in the analysis, as one of the main aspects of this work is to provide a data set ready to be used for any chemical model, for the specific area.

[34] To quantify the impact of total ozone column on JO^1D, we have plotted JO^1D at 60° sza versus total ozone (Figure 9), for low aerosol optical depth (AOD < 0.2) and weakly absorbing (non dust, $AE_{340/440} > 1$) conditions. This linear regression shows that 41% of JO^1D variability at 60° sza is explained by total ozone variability. The slope indicates a reduction of JO^1D by $4.2 \cdot 10^{-8}$ s^{-1} per total O_3 column DU. This translates to a reduction of about 30% at 60° sza, under typical spring conditions (340 DU), as compared with minimum total ozone fall conditions (280 DU). The respective slope at Lambedusa, is $3.38 \cdot 10^{-8}$ s^{-1} per total O_3 column

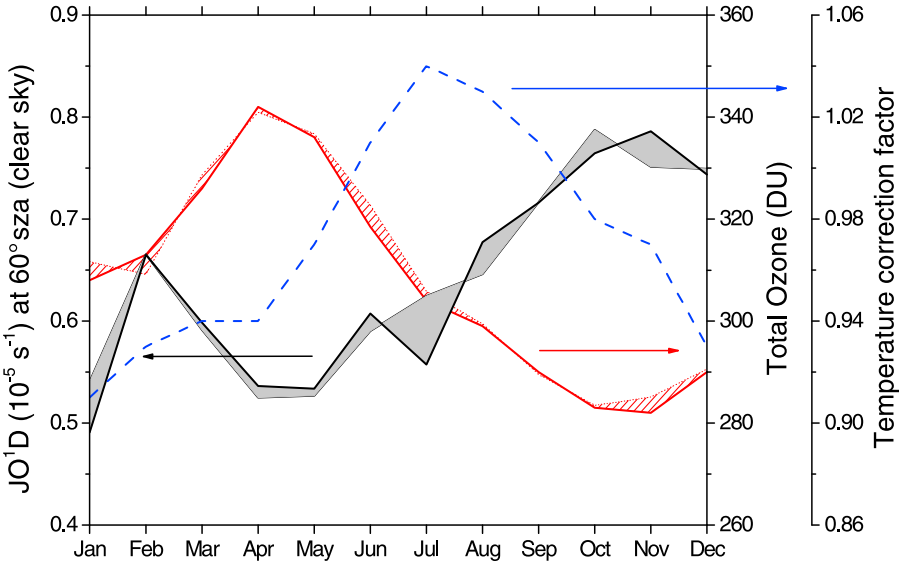

Figure 8. Seasonal cycles of the clear-sky photolysis frequency of O_3 (JO^1D) at 60° sza and total ozone column. The thick line limit of the shaded areas corresponds to median values, and the dotted line corresponds to mean values.

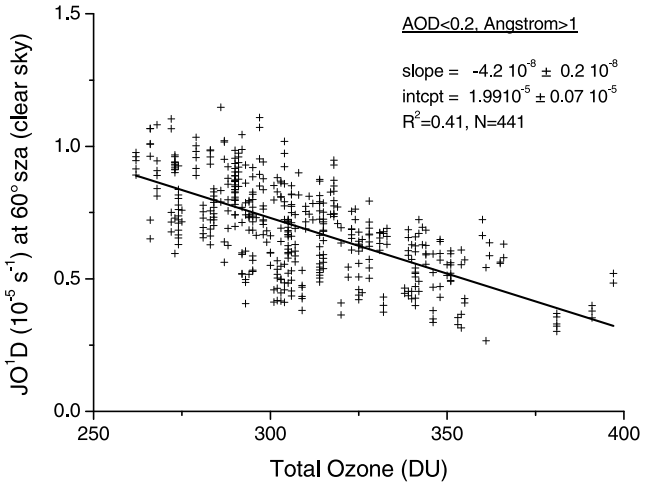

Figure 9. Photolysis frequency (clear-sky data) of O_3 (JO^1D) at 60° sza versus total ozone, for AOD < 0.2 and Angström Exponent ($AE_{340/440}$) > 1. Linear regression analysis information is included.

DU, also at 60° sza, in the AOD (416 nm) range 0.1–0.2 [*Casasanta et al.*, 2011]. The latter authors, when calculating the respective slopes for higher aerosol AOD bins, found an absence of trend, indicating that the ozone effect is essentially decoupled from the influence of aerosols.

3.2.3. Percentage Impacts of Aerosols and Ozone on Photolysis Frequencies

[35] The impact of both aerosols and total columnar ozone on JO^1D and JNO_2 was carefully studied for the case of sza of 60° encountered all year-round. In order to address aerosol and total ozone effects at all values of sza, we extended the aforementioned linear regression analysis to sza spanning the range 15° to 75° (for clear-sky conditions) in steps of 5°. We thus calculated JNO_2 and JO^1D reference values that correspond to the case AOD = 0 (the intercept of the correlation plot of Js versus AOD) for all sza. For the JO^1D reference value, the regression analyses were confined to total O_3 column of 300–320 DU since this is the most frequent distribution bin observed over the area. Note that, as mentioned earlier, the total O_3 column affects only JO^1D. We then computed the percentage difference of Js from these reference J values per sza (Figure 10). Finally, the impact of total ozone on JO^1D was confined to cases of AOD < 0.2 and $AE_{340/440}$ > 1 (relatively clear aerosol conditions with little or no dust presence) and the reference value for JO^1D having used the intercept for AOD = 0 and total ozone of 300–320 DU (Figure 10c).

[36] In Figure 10a the percentage difference of JNO_2 from the $JNO_2^{AOD=0}$ reference value is presented for four characteristic AOD levels. At regional AOD background levels (∼0.1) the percentage reduction of JNO_2 ranges between 0.3% and 6% for sza between 15° and 75°. Under typical urban conditions (AOD ∼ 0.3) the reduction is 10% at 60° sza and approaches 20% for higher sza. When considering specific high aerosol loads such as during dust events (AOD ∼ 0.5 and AOD ∼ 0.7), then the reduction at 60° sza is 17% and 24%, respectively, rising to values as high as 30%–40% for higher sza. *Ruggaber et al.* [1994] using AOD = 0.1 as a reference value, simulated that JNO_2 at 60° sza is reduced by 11%, 18% and 30% for AODs 0.3, 0.5 and 0.7, respectively (noting extrapolated values from their Figure 5b). These results are in good agreement with the observation-derived values of the present study, given the different reference value used. A similar range of JNO_2 reduction by aerosols (of the order of 10%–30%) has been calculated by *Castro et al.* [2001] using a simple zero-dimensional photochemical model. *Li et al.* [2011] also

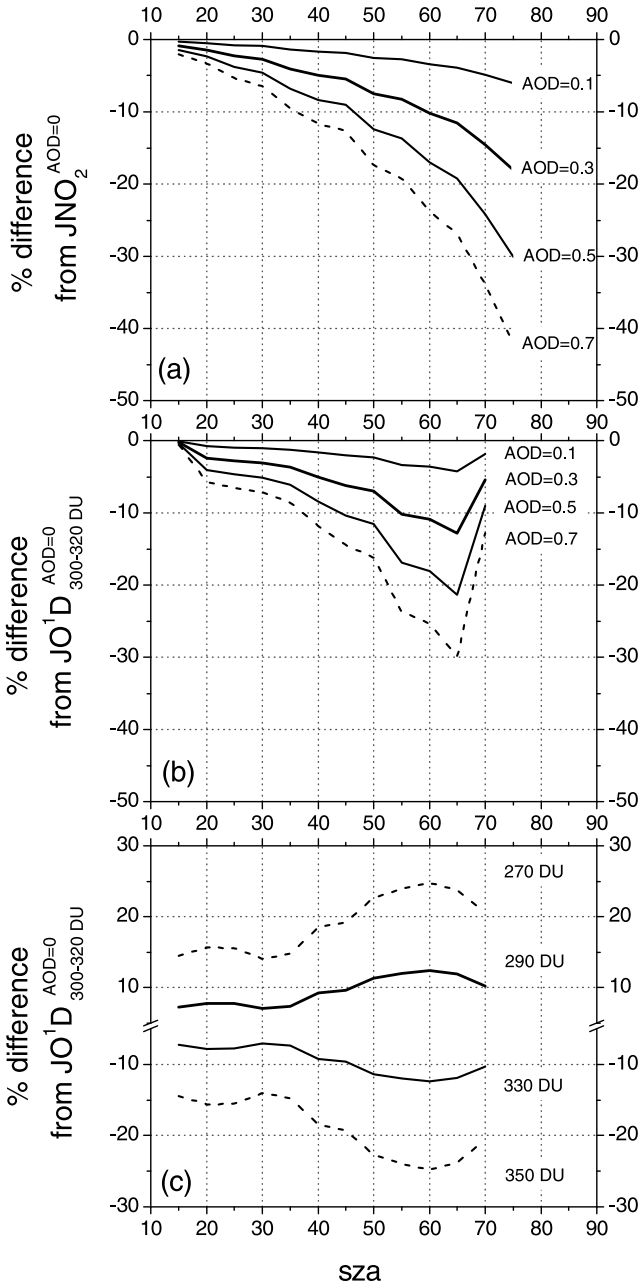

Figure 10. Percentage difference of photolysis frequencies (a) JNO_2 and (b) JO^1D, from a reference J value, per sza, for characteristic AOD (380 nm). (c) Percentage difference of JO^1D from the reference value, per sza, for typical total ozone column content. The JNO_2 reference value corresponds to AOD = 0, for each sza, while the JO^1D reference value corresponds to AOD = 0 and total ozone column in the range 300–320 DU.

Table 2. Daily Mean Values and Standard Deviations of 5 min Data Used as Input to the Chemical Box Model for Simulations A and B[a]

Data Input to the Model	Simulation A: 14 May 2004	Simulation B: 27 May 2004
Temperature (°C)	16.9 ± 0.7	16.1 ± 0.8
Relative humidity (%)	67.9 ± 0.7	68.1 ± 3.9
JO^1D (s^{-1})	$0.90 \cdot 10^{-5} \pm 1.16 \cdot 10^{-5}$	$0.70 \cdot 10^{-5} \pm 0.88 \cdot 10^{-5}$
JNO_2 (s^{-1})	$3.75 \cdot 10^{-3} \pm 3.92 \cdot 10^{-3}$	$3.52 \cdot 10^{-3} \pm 3.69 \cdot 10^{-3}$
O_3 (ppb)	45.0 ± 2.1	45.2 ± 2.4
NO_2 (ppb)	0.63 ± 0.33	0.51 ± 0.12
CO (ppb)	212.6 ± 3.0	212.6 ± 3.0
VOC reactivity against OH (s^{-1})	0.22	0.22

[a]See text. CO hourly observations have been used, while VOC reactivity against OH was kept constant throughout the simulations.

reported that in urban areas aerosols reduce JNO_2 by 1%–5% around noontime when both aerosol growth and sza decrease take place.

[37] The effect of aerosols on JO^1D is similarly shown in Figure 10b. The percentage reduction of JO^1D at 60° sza (compared to $JO^1D^{AOD=0}_{300-320\ DU}$) for AOD 0.1, 0.3, 0.5 and 0.7 is 4%, 11%, 18% and 25%, respectively. The JO^1D changes extrapolated from *Ruggaber et al.* [1994, Figure 5a], for AOD 0.3, 0.5 and 0.7, at 60° sza (using AOD = 0.1 as a reference value), and for a total ozone column content of 300 DU, are 10%, 20% and 30%, respectively, again in good agreement with the values obtained in this study, given the different AOD and total ozone reference values used. In the central Mediterranean, *Casasanta et al.* [2011] calculated a 62% and 47% reduction in JO^1D per AOD (416 nm) unit at 60° and 30° sza, respectively, whereas the values from this study are much lower in both cases (35% and 10%) . Part of the latter discrepancy might again be due to the fact that higher dust impact is expected at Lambedusa (due to its proximity to dust sources). *Li et al.* [2011] reported that in an urban area aerosols reduce JO^1D by 7%–10% around noontime. Finally, *Martin et al.* [2003], using a global three-dimensional chemical transport model (CTM), calculated a 5%–15% JO^1D reduction by aerosols at the surface, throughout most of the Northern Hemisphere. Both studies are in good agreement with the range of values provided in Figure 10b.

[38] Comparing Figures 10a and 10b it is deduced that the effect of AOD on both photolysis frequencies is similar for sza up to 65°. Figure 10b also reveals that at sza > 65°, the difference from the reference value of JO^1D decrease reflecting the fact that more photons are making it down to the Earth's surface. This is possibly due to multiple scattering that results in enhanced diffusion (especially at UV-B wavelengths) from lower sza. The same effect is at work in the work by *Ruggaber et al.* [1994] who simulated that for sza > 80°, JO^1D increases with increasing AOD. However, large errors can occur in simulations at such high sza, in particular if a plain atmosphere is assumed in the model.

[39] Finally, the effect of O_3 absorption on JO^1D is shown in Figure 10c, with respect to the absorption by a total ozone column of 300–320 DU and when AOD = 0. A general increasing trend is observed throughout the sza range. The percentage difference from the reference value increases for total ozone column <300–320 DU and decreases for total ozone column >300–320 DU. A step of 20 DU was chosen as it corresponds to typical daily variability in the amount of total ozone over the region. This is calculated as the average of the absolute difference between successive days. The percentage change in JO^1D for a deviation by 20 DU is 12% at 60° sza, while for sza < 35° it is lower (around 7.5%).

3.3. Impact of Photolysis Frequencies on Photochemistry: A Case Study

[40] In order to illustrate the impact of observed changes in photolysis frequencies on photochemistry and, in particular, on the ozone budget, we employed the chemical box model described in section 2. We chose 2 nearby days (small sza effect) having significantly different AOD values: one relatively clean (day A, 14 May 2004, $AOD_{380} = 0.2$, and air mass back trajectories indicating westerlies crossing the Mediterranean Sea), and the other having high aerosol loading (day B, 27 May 2004, $AOD_{380} = 0.41$, with air masses coming from Northern Europe and the Balkans). Total ozone columns for these 2 days is 306 and 338 DU, respectively. Under these conditions, local noon JO^1D values decreased from $3.23 \cdot 10^{-5}\ s^{-1}$ to $2.46 \cdot 10^{-5}\ s^{-1}$ (i.e., by 24%) and JNO_2 values decreased from $9.5 \cdot 10^{-3}\ s^{-1}$ to $8.98 \cdot 10^{-3}\ s^{-1}$ (i.e., by 5%). Observed 5 min interval values of O_3, NO_2, JNO_2, JO^1D, temperature, relative humidity (RH) and wind speed (from the routine measurements at Finokalia station) were used as input to the chemical box model. Hourly observations of CO for spring have also been used as input to the model. The reactivity of VOC against OH has been kept constant for both simulations. Table 2 provides the 24 h mean values of inputs to the box model. For the present study, three simulations were performed: one having Day A input data taken as the base case simulation (simulation A), a second one for which the Js of day A were replaced by the Js observed during day B (simulation AB), and the third simulation for which all 5 min averaged data inputs were replaced by those observed during day B (simulation B). The net chemical ozone production Net $[O_3]$ (in ppbv $5min^{-1}$) was then calculated using the chemical box model as explained in section 2.4.

[41] Tropospheric ozone production is fueled by peroxy radicals and requires NO_2 photodissociation as well as the availability of sufficient NO_2 as shown in the cases studied (Table 2). Therefore the reduction of JNO_2 leads to lower ozone chemical production. However, in parallel to this, a reduction of the photolysis frequency of O_3 itself (JO^1D) results in weaker O_3 loss during OH formation and subsequently an even weaker loss by reactions with HO_x. Overall, the simulations calculated a 12% reduction in the diurnal value of Net$[O_3]$ due to the weakening of the photolysis frequencies (simulation AB compared to simulation A) and a 29% overall reduction due to changes in meteorological and chemical conditions (simulation B

compared to simulation A). In particular, it is found that the reduction of Js (simulation AB versus simulation A) results to a 13% reduction in the diurnal P_{O3} and a higher (19%) reduction in the O_3 loss term due to the greater weakening of JO^1D compared to JNO_2. Similarly, the reduction of Js results in ~10% lower HO_2 and ~11% lower OH daytime concentrations. The latter is calculated by the chemical box model to be of the order of $7.5 \cdot 10^6 \pm 1.2 \cdot 10^6$ molecules cm^{-3} (daily mean), which compares well with other measurements in the region ($8.2 \cdot 10^6 \pm 1.6 \cdot 10^6$ molecule cm^{-3} [*Berresheim et al.*, 2003]). NO_3 radical concentrations are not affected since they are mainly observed during nighttime, in the absence of photochemistry, depending only on NO_z levels.

4. Summary

[42] The results highlight the need for reliable values of photolysis frequencies as drivers of (photo)chemical processes in the atmosphere, and for their evaluation with chemical transport models (CTMs). Furthermore, long-term, continuous measurements of the photolysis frequencies are scarce, especially in the eastern Mediterranean which constitutes a well recognized photochemical natural laboratory [*Kanakidou et al.*, 2011]. In this work we have presented a long-term (5-yr) study of the photolysis frequency of NO_2 (JNO_2) and ozone (JO^1D) in the eastern Mediterranean, providing explicit and detailed information on seasonal and diurnal patterns, as well as quantitative estimates of the effects of total ozone and aerosols.

[43] The key findings of this work are as follows.

[44] 1. The maximum JNO_2 occurs in May–June due to its dependence on sza, while the JO^1D seasonal maximum is shifted forward one month to July due to the reduction of total ozone from June to July that is masking the dependence of the solar actinic flux on sza.

[45] 2. The diurnal maximum of JO^1D is encountered in summer due to sza effects and columnar ozone concentrations, which are both lower in summer compared to spring. For JNO_2 maximum effect of aerosol in summer result in less profound difference of the diurnal maximum between summer and spring, under clear skies.

[46] 3. At regional aerosol background levels (AOD ~ 0.1) and average values for the content of the total ozone column, the percentage reduction of both JNO_2 and JO^1D, compared to $JNO_2^{AOD=0}$ and $JO^1D^{AOD=0}_{300-320\ DU}$, respectively, is <6% for sza between 15° and 75°. Under typical urban conditions (AOD ~ 0.3) and average total ozone column (300–320 DU), the respective percentage reduction of JNO_2 is 10% at 60° sza, approaching 20% for higher sza, while for JO^1D the percentage reduction has a maximum of 11% at 60° sza.

[47] 4. Absorption by dust is generally higher than absorption due to other prevailing aerosols in the region. During episodes of high aerosol loads, e.g., during dust events, at 60° sza the percentage reduction of JNO_2, compared to the reference value, is 17% and 24%, for AOD ~ 0.5 and AOD ~ 0.7, respectively, reaching as much as 30%–40% for higher sza. The reductions in JO^1D at 60° sza are 18% and 25%, respectively.

[48] 5. For the whole 5-yr period, and for an average AOD (380 nm) value of 0.27 ± 0.13 (1-sigma standard deviation) over Island of Crete, we obtained a reduction in JNO_2 ranging between 5% and 14%, at 60° sza, compared to aerosol-free conditions. Furthermore, for the average total ozone column (300–320 DU), the respective range of JO^1D reduction was found to be 5%–15%. A daily variability of 20 DU in total ozone column over the region, resulted in a change in JO^1D of 12% at 60° sza, while for sza < 35° it was found to be lower (around 7.5%).

[49] 6. Finally, a reduction of Js corresponding to a 24% decrease in the local noon JO^1D value and a 5% decrease in the local noon JNO_2 value, was found to result in a 12% reduction in the 24 h mean Net[O_3] due only to the weakening of the photolysis frequencies and a 29% overall reduction due to changes in both meteorological and chemical conditions.

[50] **Acknowledgments.** This study was conducted within the framework of the CIRCE Project (Climate Change and Impact Research: The Mediterranean Environment, http://www.circeproject.eu/), funded by the Commission of the European Union (contract 036961 GOCE). S.K. would like to acknowledge ACI-UV (FP7-PEOPLE-2009-RG Marie Curie European Reintegration Grant, PERG05-GA-2009-247492). M.V. acknowledges the PARTHENO$_2$N Project (FP7-PEOPLE-2009-RG Marie Curie European Reintegration Grant, PERG-GA-2009-256391). The authors would like to thank the Research Account of the University of Crete for financial support.

References

Anderson, G. P., S. A. Clough, F. X. Kneizys, J. H. Chetwynd, and E. P. Shettle (1986), AFGL atmospheric constituent profiles (0–120 km), *Tech. Rep. AFGL-TR-86-0110*, Air Force Geophys. Lab., Hanscom Air Force Base, Mass.

Atkinson, R., D. L. Baulch, R. A. Cox, J. N. Crowley, R. F. Hampson, R. G. Hynes, M. E. Jenkin, M. J. Rossi, and J. Troe (2004), Evaluated kinetic and photochemical data for atmospheric chemistry: Volume I—Gas phase reactions of O_x, HO_x, NO_x and SO_x species, *Atmos. Chem. Phys.*, *4*, 1461–1738, doi:10.5194/acp-4-1461-2004.

Bahe, F. C., W. N. Marx, U. Schurath, and E. Roth (1979), Determination of the absolute photolysis rate of ozone by sunlight, $O_3 + h\nu \rightarrow O(^1D) + O_2(^1\Delta g)$, at ground level, *Atmos. Environ.*, *13*, 1515–1522, doi:10.1016/0004-6981(79)90060-X.

Bais, A. F., et al. (2003), International photolysis frequency measurement and model intercomparison: Spectral actinic solar flux measurements and modeling, *J. Geophys. Res.*, *108*(D16), 8543, doi:10.1029/2002JD002891.

Balis, D. S., C. S. Zerefos, K. Kourtidis, A. F. Bais, A. Hofzumahaus, A. Kraus, R. Schmitt, M. Blumthaler, and G. P. Gobbi (2002), Measurements and modeling of photolysis rates the Photochemical Activity and Ultraviolet Radiation (PAUR) II campaign, *J. Geophys. Res.*, *107*(D18), 8138, doi:10.1029/2000JD000136.

Balis, D. S., et al. (2004), Study of the effect of different type of aerosols on UV-B radiation from measurements during EARLINET, *Atmos. Chem. Phys.*, *4*, 307–321, doi:10.5194/acp-4-307-2004.

Berresheim, H., C. Plass-Dülmer, T. Elste, N. Mihalopoulos, and F. Rohrer (2003), OH in the coastal boundary layer of Crete during MINOS: Measurements and relationship with ozone photolysis, *Atmos. Chem. Phys.*, *3*, 639–649, doi:10.5194/acp-3-639-2003.

Bian, H., and C. S. Zender (2003), Mineral dust and global tropospheric chemistry: Relative roles of photolysis and heterogeneous uptake, *J. Geophys. Res.*, *108*(D21), 4672, doi:10.1029/2002JD003143.

Bohn, B., A. Kraus, M. Müller, and A. Hofzumahaus (2004), Measurement of atmospheric $O_3 \rightarrow O(^1D)$ photolysis frequencies using filter radiometry, *J. Geophys. Res.*, *109*, D10S90, doi:10.1029/2003JD004319.

Bohn, B., et al. (2008), Photolysis frequency measurement techniques: Results of a comparison within the ACCENT project, *Atmos. Chem. Phys.*, *8*, 5373–5391, doi:10.5194/acp-8-5373-2008.

Casasanta, G., A. di Sarra, D. Meloni, F. Monteleone, G. Pace, S. Piacentino, and D. Sferlazzo (2011), Large aerosol effects on ozone photolysis in the Mediterranean, *Atmos. Environ.*, *45*, 3937–3943, doi:10.1016/j.atmosenv.2011.04.065.

Castro, T., S. Madronich, S. Rivale, A. Muhlia, and B. Mar (2001), The influence of aerosols on photochemical smog in Mexico City, *Atmos. Environ.*, *35*, 1765–1772, doi:10.1016/S1352-2310(00)00449-0.

Crutzen, P. J. (1995), Ozone in the troposphere, in *Composition, Chemistry, and Climate of the Atmosphere*, edited by H. B. Singh, pp. 349–393, Van Nostrand Reinold, New York.

Dickerson, R. R., D. H. Stedman, W. L. Chameides, P. J. Crutzen, and J. Fishman (1979), Actinometric measurements and theoretical calculations of $j(O_3)$, the rate of photolysis of ozone to $O(^1D)$, *Geophys. Res. Lett.*, *6*, 833–836, doi:10.1029/GL006i011p00833.

Dickerson, R. R., S. Kondragunta, G. Stenchikov, K. L. Civerolo, B. G. Doddridge, and B. N. Holben (1997), The impact of aerosols on solar ultraviolet radiation and photochemical smog, *Science*, *278*, 827–830, doi:10.1126/science.278.5339.827.

Dubovik, O., and M. D. King (2000), A flexible inversion algorithm for retrieval of aerosol optical properties from Sun and sky radiance measurements, *J. Geophys. Res.*, *105*, 20,673–20,696, doi:10.1029/2000JD900282.

Ehhalt, D. H., and F. Rohrer (2000), Dependence of the OH concentration on solar UV, *J. Geophys. Res.*, *105*(D3), 3565–3571, doi:10.1029/1999JD901070.

Finlayson-Pitts, B. J., and J. N. Pitts (2000), *Chemistry of the Upper and Lower Atmosphere*, Academic, San Diego, Calif.

Fotiadi, A., N. Hatzianastassiou, E. Drakakis, C. Matsoukas, K. G. Pavlakis, D. Hatzidimitriou, E. Gerasopoulos, N. Mihalopoulos, and I. Vardavas (2006), Aerosol physical and optical properties in the eastern Mediterranean Basin, Crete, from Aerosol Robotic Network data, *Atmos. Chem. Phys.*, *6*, 5399–5413, doi:10.5194/acp-6-5399-2006.

Gerasopoulos, E., G. Kouvarakis, M. Vrekoussis, M. Kanakidou, and N. Mihalopoulos (2005), Ozone variability in the marine boundary layer of the eastern Mediterranean based on 7-year observations, *J. Geophys. Res.*, *110*, D15309, doi:10.1029/2005JD005991.

Gerasopoulos, E., G. Kouvarakis, M. Vrekoussis, C. Donoussis, N. Mihalopoulos, and M. Kanakidou (2006), Photochemical ozone production in the eastern Mediterranean, *Atmos. Environ.*, *40*, 3057–3069, doi:10.1016/j.atmosenv.2005.12.061.

Gerasopoulos, E., V. Amiridis, S. Kazadzis, P. Kokkalis, K. Eleftheratos, M. O. Andreae, T. W. Andreae, H. El-Askary, and C. S. Zerefos (2011), Three-year ground based measurements of aerosol optical depth over the eastern Mediterranean: The urban environment of Athens, *Atmos. Chem. Phys.*, *11*, 2145–2159, doi:10.5194/acp-11-2145-2011.

He, S., and G. R. Carmichael (1999), Sensitivity of photolysis rates and ozone production in the troposphere to aerosol properties, *J. Geophys. Res.*, *104*, 26,307–26,324, doi:10.1029/1999JD900789.

Hofzumahaus, A., A. Kraus, A. Kylling, and C. S. Zerefos (2002), Solar actinic radiation (280–420 nm) in the cloud-free troposphere between ground and 12 km altitude: Measurements and model results, *J. Geophys. Res.*, *107*(D18), 8139, doi:10.1029/2001JD900142.

Hofzumahaus, A., et al. (2004), Photolysis frequency of O_3 to $O(^1D)$: Measurement and modeling during the International Photolysis Frequency Measurement and Modeling Intercomparison (IPMMI), *J. Geophys. Res.*, *109*, D08S90, doi:10.1029/2003JD004333.

Holland, F., A. Hofzumahaus, J. Schäfer, A. Kraus, and H.-W. Pätz (2003), Measurements of OH and HO_2 radical concentrations and photolysis frequencies during BERLIOZ, *J. Geophys. Res.*, *108*(D4), 8246, doi:10.1029/2001JD001393.

Hudson, R. D., A. D. Frolov, M. F. Andrade, and M. B. Follette (2003), The total ozone field separated into meteorological regimes. Part I: Defining the regimes, *J. Atmos. Sci.*, *60*, 1669–1677, doi:10.1175/1520-0469(2003)060<1669:TTOFSI>2.0.CO;2.

Jacob, D. J., J. H. Crawford, M. M. Kleb, V. S. Connors, R. J. Bendura, J. L. Raper Jr., G. W. Sachse, J. C. Gille, L. Emmons and C. L. Heald (2003), Transport and Chemical Evolution over the Pacific (TRACE-P) mission: Design, execution, and first results, *J. Geophys. Res.*, *108*(D20), 9000, doi:10.1029/2002JD003276.

Jacobson, M. Z. (1998), Studying the effects of aerosols on vertical photolysis rate coefficient and temperature profiles over an urban airshed, *J. Geophys. Res.*, *103*, 10,593–10,604, doi:10.1029/98JD00287.

Junkermann, W., U. Platt, and A. Volz-Thomas (1989), A photoelectric detector for the measurement of photolysis frequencies of ozone and other atmospheric molecules, *J. Atmos. Chem.*, *8*, 203–227, doi:10.1007/BF00051494.

Kanakidou, M., and P. J. Crutzen (1999), The photochemical source of carbon monoxide: Importance, uncertainties and feedbacks, *Chemosphere Global Change Sci.*, *1*, 91–109, doi:10.1016/S1465-9972(99)00022-7.

Kanakidou, M., et al. (2011), Megacities as hot spots of air pollution in the East Mediterranean, *Atmos. Environ.*, *45*, 1223–1235, doi:10.1016/j.atmosenv.2010.11.048.

Kazadzis, S., C. Topaloglou, A. F. Bais, M. Blumthaler, D. Balis, A. Kazantzidis, and B. Schallhart (2004), Actinic flux and O^1D photolysis frequencies retrieved from spectral measurements of irradiance at Thessaloniki, Greece, *Atmos. Chem. Phys.*, *4*, 2215–2226, doi:10.5194/acp-4-2215-2004.

Kraus, A., and A. Hofzumahaus (1998), Field measurements of atmospheric photolysis frequencies for O_3, NO_2, HCHO, H_2O_2 and HONO by UV spectroradiometry, *J. Atmos. Chem.*, *31*, 161–180, doi:10.1023/A:1005888220949.

Li, G., N. Bei, X. Tie, and L. T. Molina (2011), Aerosol effects on the photochemistry in Mexico City during MCMA-2006/MILAGRO campaign, *Atmos. Chem. Phys.*, *11*, 5169–5182, doi:10.5194/acp-11-5169-2011.

Liakakou, E., M. Vrekoussis, B. Bonsang, C. Donousis, M. Kanakidou, and N. Mihalopoulos (2007), Isoprene above the eastern Mediterranean: Seasonal variation and contribution to the oxidation capacity of the atmosphere, *Atmos. Environ.*, *41*, 1002–1010, doi:10.1016/j.atmosenv.2006.09.034.

Liakakou, E., B. Bonsang, J. Williams, N. Kalivitis, M. Kanakidou, and N. Mihalopoulos (2009), C_2–C_8 NMHCs over the eastern Mediterranean: Seasonal variation and impact on regional oxidation chemistry, *Atmos. Environ.*, *43*, 5611–5621, doi:10.1016/j.atmosenv.2009.07.067.

Liao, H., Y. L. Yung, and J. H. Seinfeld (1999), Effects of aerosols on tropospheric photolysis rates in clear and cloudy atmospheres, *J. Geophys. Res.*, *104*, 23,697–23,707, doi:10.1029/1999JD900409.

Liao, H., P. J. Adams, S. H. Chung, J. H. Seinfeld, L. J. Mickley, and D. J. Jacob (2003), Interactions between tropospheric chemistry and aerosols in a unified general circulation model, *J. Geophys. Res.*, *108*(D1), 4001, doi:10.1029/2001JD001260.

Madronich, S. (1987), Photodissociation in the atmosphere: 1. Actinic flux and the effects of ground reflections and clouds, *J. Geophys. Res.*, *92*, 9740–9752, doi:10.1029/JD092iD08p09740.

Malicet, J., D. Daumont, J. Charbonnier, C. Parisse, A. Chakir, and J. Brion (1995), Ozone UV spectroscopy. II. Absorption cross-sections and temperature dependence, *J. Atmos. Chem.*, *21*, 263–273, doi:10.1007/BF00696758.

Martin, R. V., D. J. Jacob, R. M. Yantosca, M. Chin, and P. Ginoux (2003), Global and regional decreases in tropospheric oxidants from photochemical effects of aerosols, *J. Geophys. Res.*, *108*(D3), 4097, doi:10.1029/2002JD002622.

Matsumi, Y., F. J. Comes, G. Hancock, A. Hofzumahaus, A. J. Hynes, M. Kawasaki, and A. R. Ravishankara (2002), Quantum yields for production of $O(^1D)$ in the ultraviolet photolysis of ozone: Recommendation based on evaluation of laboratory data, *J. Geophys. Res.*, *107*(D3), 4024, doi:10.1029/2001JD000510.

Mayer, B., and A. Kylling (2005), Technical note: The libRadtran software package for radiative transfer calculations—Description and examples of use, *Atmos. Chem. Phys.*, *5*, 1855–1877, doi:10.5194/acp-5-1855-2005.

Mihalopoulos, N., E. Stephanou, S. Pilitsidis, M. Kanakidou, and P. Bousquet (1997), Atmospheric aerosol composition above the eastern Mediterranean region, *Tellus, Ser. B*, *49*, 314–326.

Molina, L. T., et al. (2010), An overview of the MILAGRO 2006 Campaign: Mexico City emissions and their transport and transformation, *Atmos. Chem. Phys.*, *10*, 8697–8760, doi:10.5194/acp-10-8697-2010.

Müller, M., A. Kraus, and A. Hofzumahaus (1995), O_3 $O(^1D)$ photolysis frequencies determined from spectroradiometric measurements of solar actinic UV-radiation: Comparison with chemical actinometer measurements, *Geophys. Res. Lett.*, *22*, 679–682, doi:10.1029/95GL00203.

Plass-Dülmer, C., M. Ratte, R. Koppmann, and J. Rudolph (1992), C_2–C_9 hydrocarbons in the marine atmosphere during NATAC 91, paper presented at the NATAC 91 Workshop, Natl. Aerospace Technol. Advis. Comm., Odessa, Ukraine.

Plass-Dülmer, C., T. Brauers, and J. Rudolph (1998), POPCORN: A field study of photochemistry in north-eastern Germany, *J. Atmos. Chem.*, *31*, 5–31, doi:10.1023/A:1006098202013.

Poisson, N., et al. (2001), The impact of natural non-methane hydrocarbon oxidation on the free radical and ozone budgets above a eucalyptus forest, *Chemosphere Global Change Sci.*, *3*, 353–366, doi:10.1016/S1465-9972(01)00016-2.

Querol, X., A. Alastuey, J. Pey, M. Cusack, N. Perez, N. Mihalopoulos, C. Theodosi, E. Gerasopoulos, N. Kubilay, and M. Kocak (2009), Variability in regional background aerosols within the Mediterranean, *Atmos. Chem. Phys.*, *9*, 4575–4591, doi:10.5194/acp-9-4575-2009.

Rohrer, F., and H. Berresheim (2006), Strong correlation between levels of tropospheric hydroxyl radicals and solar ultraviolet radiation, *Nature*, *442*, 184–187, doi:10.1038/nature04924.

Ruggaber, A., R. Dlugi, and T. Nakajima (1994), Modelling radiation quantities and photolysis frequencies in the troposphere, *J. Atmos. Chem.*, *18*, 171–210, doi:10.1007/BF00696813.

Shettle, E. P. (1989), Models of aerosols, clouds and precipitation for atmospheric propagation studies, in *Atmospheric Propagation in the UV, Visible, IR and MM-Wave Region and Related System Aspects*, *AGARD Conf. Proc.*, *454*, 26 pp., Neuilly sur Seine, France.

Topaloglou, C., S. Kazadzis, A. F. Bais, M. Blumthaler, B. Schallhart, and D. Balis (2005), NO_2 and HCHO photolysis frequencies from irradiance measurements in Thessaloniki, Greece, *Atmos. Chem. Phys.*, *5*, 1645–1653, doi:10.5194/acp-5-1645-2005.

Troe, J. (2000), Are primary quantum yields of NO_2 photolysis at $\lambda \leq$ 398 nm smaller than unity?, *Z. Phys. Chem.*, *214*, 573–581, doi:10.1524/zpch.2000.214.5.573.

Tsigaridis, K., and M. Kanakidou (2002), Importance of volatile organic compounds photochemistry over a forested area in central Greece, *Atmos. Environ.*, *36*, 3137–3146, doi:10.1016/S1352-2310(02)00234-0.

Vandaele, A. C., C. Hermans, S. Fally, M. Carleer, M. F. Merienne, A. Jenouvrier, B. Coquart, and R. Colin (2003), Absorption cross-sections of NO_2: Simulation of temperature and pressure effects, *J. Quant. Spectrosc. Radiat. Transf.*, *76*, 373–391, doi:10.1016/S0022-4073(02)00064-X.

Volz-Thomas, A., A. Lerner, H.-W. Platz, M. Schultz, D. S. McKenna, R. Schmitt, S. Madronich, and E. P. Röth (1996), Airborne measurements of the photolysis frequency of NO_2, *J. Geophys. Res.*, *101*, 18,613–18,627, doi:10.1029/96JD01375.

Vrekoussis, M., M. Kanakidou, N. Mihalopoulos, P. J. Crutzen, J. Lelieveld, D. Perner, H. Berresheim, and E. Baboukas (2004), Role of the NO_3 radicals in oxidation processes in the eastern Mediterranean troposphere during the MINOS campaign, *Atmos. Chem. Phys.*, *4*, 169–182, doi:10.5194/acp-4-169-2004.

Vrekoussis, M., E. Liakakou, N. Mihalopoulos, M. Kanakidou, P. J. Crutzen, and J. Lelieveld (2006), Formation of HNO_3 and NO_3 in the anthropogenically influenced eastern Mediterranean marine boundary layer, *Geophys. Res. Lett.*, *33*, L05811, doi:10.1029/2005GL025069.

Webb, A. R., R. Kift, S. Thiel, and M. Blumthaler (2002), An empirical method for the conversion of spectral UV irradiance measurements to actinic flux data, *Atmos. Environ.*, *36*, 4397–4404, doi:10.1016/S1352-2310(02)00319-9.

Zanis, P., P. S. Monks, E. Schuepbach, and S. A. Penkett (1999), On the relationship of HO_2 + RO_2 with $J(O^1D)$ during FREETEX '96 at the Jungfraujoch Observatory (3580 m above sea level) in the Swiss Alps, *J. Geophys. Res.*, *104*, 26,913–26,926, doi:10.1029/1999JD900282.

Zanis, P., P. S. Monks, E. Schuepbach, L. J. Carpenter, T. J. Green, G. P. Mills, S. Bauguitte, and S. A. Penkett (2000), In situ ozone production under free tropospheric conditions during FREETEX '98 in the Swiss Alps, *J. Geophys. Res.*, *105*, 24,223–24,234, doi:10.1029/2000JD900229.

Zanis, P., K. Kourtidis, B. Rappenglueck, C. Zerefos, D. Melas, D. Balis, R. Schmitt, S. Rapsomanikis, and P. Fabian (2002), A case study on the possible link between surface ozone photochemistry and total ozone column during the PAUR II experiment at Crete: Comparison of observations with box model calculations, *J. Geophys. Res.*, *107*(D18), 8136, doi:10.1029/2000JD000137.

Zerefos, C. S., et al. (1998), Overview of results from PAUR campaign, paper presented at European Conference on Atmospheric UV Radiation, Eur. Comm. and Finn. Meteorol. Inst., Helsinki.

Zerefos, C. S., et al. (2002), Photochemical Activity and Solar Ultraviolet Radiation (PAUR) Modulation Factors: An overview of the project, *J. Geophys. Res.*, *107*(D18), 8134, doi:10.1029/2000JD000134.